

## SULFIDE-FACIES IRON FORMATION AT THE ARCHEAN MORLEY OCCURRENCE, NORTHWESTERN ONTARIO: CONTRASTS WITH OCEANIC HYDROTHERMAL DEPOSITS

PHILIP W. FRALICK

*Department of Geology, Lakehead University, Thunder Bay, Ontario P7B 5E1*

TIMOTHY J. BARRETT

*Mineral Exploration Research Institute, Department of Geological Sciences, McGill University,  
Montreal, Quebec H3A 2A7*

KYM E. JARVIS

*Department of Chemistry, University of Surrey, Guildford, Surrey, England GU2 5XH*

IAN JARVIS

*School of Geological Sciences, Kingston Polytechnic, Kingston-on Thames, Surrey, England KT1 2EE*

BERNIE R. SCHNIEDERS

*Ontario Ministry of Northern Development and Mines, Thunder Bay, Ontario P7C 5G3*

RONALD VANDE KEMP

*Department of Geology, Lakehead University, Thunder Bay, Ontario P7B 5E1*

### ABSTRACT

A late Archean arc-type volcanic sequence on the north shore of Lake Superior contains thin successions of sulfide-facies iron formation. One such occurrence, the  $\approx 5$  m-thick Morley deposit, consists of interlayered chert, massive and laminated pyrite layers (cm scale), and carbonaceous mudstone. Pyrite laminations are up to 1 mm thick and generally contain increased amounts of chert, carbon and detrital mud toward their tops. The laminations commonly are organized into upward-thinning cycles over  $\approx 1$  cm. Discordant pyrite growth-structures on domes, together with inclined pyrite crusts and microslumps, indicate that pyrite accumulation produced an irregular microrelief on the seafloor. Pyritic and chert layers have very low trace and rare-earth-element (*REE*) contents. *REE* patterns of pyrite samples have small positive Eu and La anomalies relative to Archean shale, whereas the chert only has a La anomaly. A modest hydrothermal signal appears to be preserved in the pyritic sediments. Sulfur isotope ratios of sulfides and whole rocks from the Morley occurrence can be accounted for by hydrothermal leaching of magmatic sulfide from the host volcanic rocks, together with a component of heavier sulfur derived from the reduction of seawater sulfate. We interpret each lamination in the pyritic beds as reflecting a short-term hydrothermal injection into a stagnant bottom layer of water. Upward-thinning cycles of laminations, indicative of gradual, but oscillatory waning of precipitation, correspond to medium-term hydrothermal events. The domal to irregular structures of the Morley pyrite provide evidence for the existence of relatively deep-water organic mats during chemical precipitation. The carbon in the pyrite laminations and associated mudstones is interpreted as a relic of this organic activity, which may have been localized around hydrothermal vents. The pyritic layers in the

Morley deposit seem most analogous to sulfidic sediments in the Red Sea brine deeps in terms of their finely laminated nature and sulfur isotope and *REE* compositions, but differ in their monomineralic nature and possibly biogenic structures.

*Keywords:* iron formation, sulfide facies, pyrite, chert, geochemistry, rare-earth elements, sulfur isotopes, oceanic hydrothermal deposits, Archean, Morley deposit, Ontario.

### SOMMAIRE

Une séquence volcanique de type arc insulaire d'âge archéen tardif sur la côte nord du lac Supérieur contient de minces couches d'un facies sulfuré d'une formation de fer. Au site du gîte de Morley, cette unité, d'une épaisseur de 5 m, contient une séquence interlitée de chert, des niveaux centimétriques de pyrite massive ou laminée, et une argile carbonacée. Les laminations de pyrite atteignent une épaisseur de 1 mm et contiennent des concentrations plus élevées de chert, de carbone et de matériel détritique vers le haut. L'épaisseur des laminations diminue généralement vers le haut en cycles étalés sur une échelle centimétrique. Des structures discordantes de croissance de la pyrite sur des dômes, ainsi que des croûtes inclinées et des micro-affaissements montrent que l'accumulation de la pyrite avait produit un microrelief sur le fond marin. Les niveaux de chert et de pyrite possèdent des teneurs en terres rares et autres éléments-traces très faibles. Les spectres de terres rares des échantillons de pyrite, normalisés avec un shale archéen moyen, révèlent des anomalies légèrement positives en Eu et La, tandis que le chert ne montre que l'anomalie en La. L'indice d'une influence hydrothermale modérée est conservé dans les sédiments pyriteux. Le rapport des

isotopes de soufre des sulfures et des roches totales à Morley reflèterait un lessivage hydrothermal de sulfures magmatiques des roches-hôtes volcaniques, et une contribution de soufre plus lourd dérivé par réduction du sulfate de l'eau de mer. Chacune des laminations de pyrite serait l'expression d'une pulsation hydrothermale injectée dans un bassin fermé d'eau stagnante. Les cycles de laminations à épaisseur qui diminue vers le haut sont une indication d'une réduction progressive mais aussi oscillatoire de la précipitation, qui correspondrait aux événements à moyen terme. Les structures en dômes ou irrégulières laissent entrevoir l'existence d'agrégats organiques à de grandes profondeurs au cours de la précipitation chimique. Le carbone dans les laminations de pyrite et les shales associés serait hérité de cette activité organique, localisée près des événements. Les niveaux de pyrite du gîte de Morley ressemblent beaucoup aux sédiments sulfurés déposés dans les bassins de saumure de la mer Rouge, surtout en termes de leur laminations fines, leurs rapports isotopiques et leurs teneurs en terres rares, mais ils diffèrent de ceux-ci par leur caractère monominéral et la présence possible de structures biogéniques.

(Traduit par la Rédaction)

**Mots-clés:** formation de fer, facies sulfuré, pyrite, chert, géochimie, terres rares, isotopes du soufre, dépôts hydrothermaux marins, archéen, gîte Morley, Ontario.

## INTRODUCTION

Iron formations, chemical sedimentary rocks containing greater than 15% Fe (James 1966), are a common lithofacies in Precambrian successions but are found only rarely in the Phanerozoic. The Precambrian iron formations can be classified into two main groups, those of Superior type, which were deposited as thick, laterally extensive units in tectonically stable areas, with sedimentary structures and textures indicative of shallow-water environments, and those of Algoma type, which accumulated in tectonically active regions as well-layered but discontinuous units, mainly in association with volcanic rocks or deep-water sediments (Gross 1965, 1983). For the Algoma type in particular, a stratigraphic-geochemical subdivision into oxide, carbonate and sulfide facies commonly can be applied (Goodwin 1964). In the present paper, we examine an unusually well-preserved pyrite-chert-rich deposit within a late Archean volcanic suite north of Lake Superior (Fig.1). Sedimentological, petrographic and geochemical data allow inferences about the nature of chemical precipitation for this particular deposit.

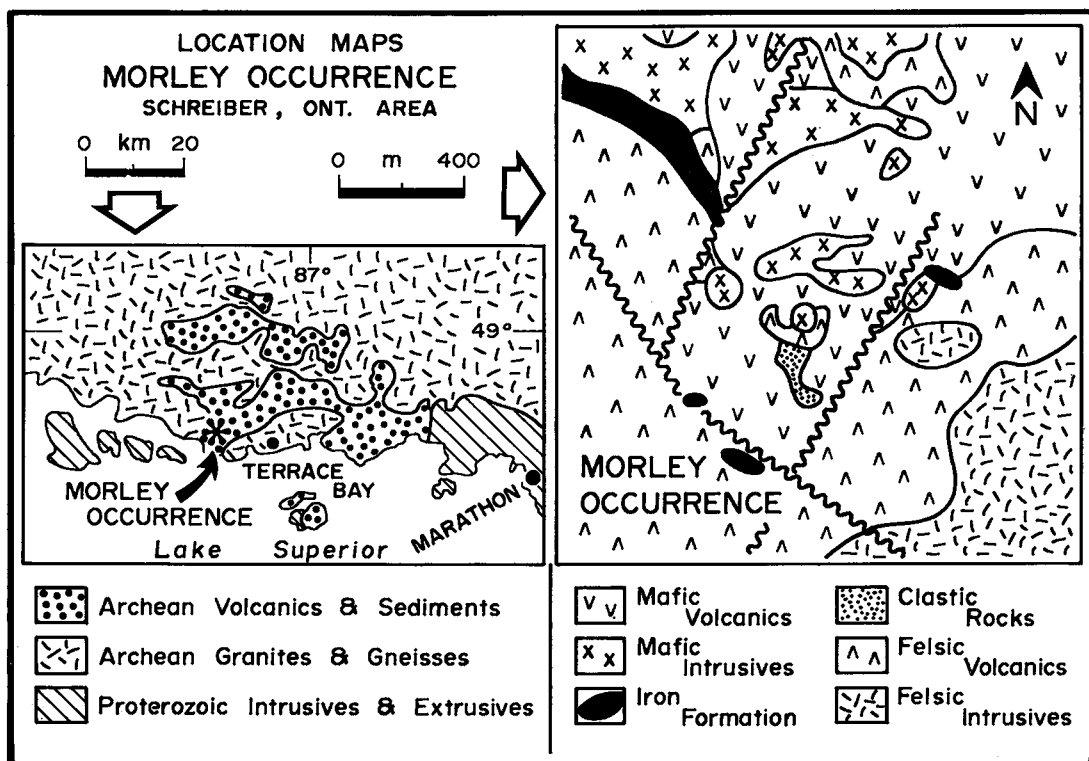


FIG. 1. Location map of the Morley pyrite occurrence. Local geology after Harcourt & Bartley (1939).

## METHODS

Samples were analyzed for major elements by X-ray fluorescence (XRF) and for trace elements by inductively coupled plasma (ICP). Sulfur isotope analyses were performed following direct combustion or Kiba extraction techniques at the Geological Survey of Canada in Ottawa (W. Carrigan, analyst), and the University of California at Los Angeles (H. Strauss, analyst). The scanning electron photomicrographs were produced using a Hitachi S-570 SEM operated at 20 kV and a take-off angle of 18°. Mineralogical identifications were made on the basis of peaks identified using a Tracor Northern 5502 energy-dispersion system (EDS).

For rare-earth-element analysis, dissolutions and extractions were performed at Kingston Polytechnic by IJ, with ICP-mass spectrometric analysis carried out at the University of Surrey by KEJ. The digestion method used was a sequential attack of aqua regia, HF-HClO<sub>3</sub>, HClO<sub>4</sub>, and finally HCl to give a final matrix of 1M HCl. Residues were filtered, ashed, and fused with lithium metaborate. The fusion was digested in HNO<sub>3</sub>, evaporated, and taken up in an aliquot of the main solution (1M HCl). The REE were extracted from the combined solutions using the method of Jarvis & Jarvis (1985). The ICP mass spectrometric technique is described in Jarvis (1988). An international standard, SCo-1, was dissolved and extracted with the unknowns, and is given in Table 1 for comparison. Interelement corrections and blank corrections were made for all samples. Blank corrections for the samples with the

lowest REE concentrations were substantial. MP-14A(R) is a replicate of MP-14A (Table 1), and was processed with a different batch of REE separations. This sample has relatively low REE concentrations. Although the blank corrections of the replicate were different (higher) than for the original sample, the corrected pattern for the replicate is in close agreement with that of MP-14A. Although some of the low-concentration samples have unusually high La contents, these anomalies appear to be real and not an analytical artifact.

## SEDIMENTOLOGY AND PETROGRAPHY

The stratigraphic sequence containing the sulfide-facies iron formation was deposited about 2.7 Ga years ago and represents a large, multicyclic arc-type volcanic edifice (Schnieders 1987). The Morley deposit, which is exposed by surface trenching, is a lenticular chemical sedimentary unit up to ≈ 5 m thick that is underlain by intermediate flows and pyroclastic rocks, and overlain by minor turbidites and mafic flows (Fig. 2). Because of the poor surface exposure and very limited drilling in the area, it is not possible to assess features such as host-rock alteration or hydrothermal supply-zones to the Morley deposit. The chemical precipitates of the deposit formed during a hiatus in eruptive activity, with pyrite and interbanded light and dark chert in the lower part of the chemical unit, and bedded to laminated pyrite in the upper part. Black, carbonaceous mudstone and thin-bedded fine-grained (DE) turbidites also are present. Within the pyrite-rich upper part of the sequence, a variety of bedding structures is developed; one five cm-thick section (right side of Fig. 2) was investigated in detail.

The upper pyritic unit contains cm-scale layers of pyrite separated by mm-scale layers of carbonaceous cherty mudstone (Figs. 3A-C). The pyrite layers contain delicate internal laminations of pyrite and carbonaceous chert from 0.02 to 1 mm thick (Figs. 3-6). Near the tops of individual pyrite laminations, the proportion of chert and disseminated clastic debris is greater (Figs. 4, 5). The mm-scale mudstone layers drape irregular pyritic surfaces, thin over colloform pyrite domes and thicken in flanking depressions. Commonly the mudstone layers thin to partings only a few hundred micrometers thick, or pinch out entirely where the top of a pyrite dome contacts the base of the overlying pyrite layer. Thin section and EDS data indicate that the mudstone layers contain quartz, muscovite, albite, carbonate, chlorite, disseminated pyrite, iron oxides and carbon.

The largest colloform pyrite dome observed is 2.5 cm high by 5 cm long, and contains about 60 pyrite laminations (Fig. 3D). The outer half of this dome is separated from underlying (and concordant) laminations by a 0.4-mm band of carbonaceous mud-

TABLE 1. MAJOR- AND TRACE-ELEMENT COMPOSITION OF PYRITIC SULFIDES AND ASSOCIATED LITHOLOGIES, MORLEY OCCURRENCE, NORTHWESTERN ONTARIO

%	MP10A light chert	MP10B dark chert	MP11 ash	MP12 turb. slate	MP13 cherty mudst.	MP14A pyrite	MP14B pyrite	MP14C pyrite	MP14D pyrite
SiO <sub>2</sub>	99.44	99.49	64.06	66.69	86.04	13.34	8.41	9.17	6.09
TiO <sub>2</sub>	0.03	0.03	0.94	0.56	0.20	0.07	0.05	0.06	0.09
Al <sub>2</sub> O <sub>3</sub>	<0.1	0.01	16.76	14.84	5.74	1.82	1.50	1.65	2.08
FeO	0.03	0.04	4.37	4.12	3.69	50.40	53.90	53.53	55.85
MnO	0.01	0.01	0.13	0.11	0.03	0.01	0.02	0.02	0.02
MgO	<0.1	0.01	2.75	2.55	0.22	0.14	0.25	0.23	0.21
CaO	0.06	0.13	0.28	3.11	0.08	0.32	0.16	0.10	0.07
Na <sub>2</sub> O	<0.1	<0.1	1.57	2.32	0.24	0.31	0.41	0.55	0.52
K <sub>2</sub> O	<0.1	<0.1	3.57	2.29	1.35	0.01	0.16	0.19	0.33
P <sub>2</sub> O <sub>5</sub>	0.01	<0.1	0.20	0.14	0.04	0.01	0.02	0.02	0.02
LOI	0.18	0.32	4.81	2.93	1.97	29.03	30.34	29.78	30.62
Total	99.76	100.04	99.44	99.46	99.60	95.66	95.22	95.30	95.90
ppm									
Se	2	75	7	5	2	64	74	74	78
Hg	bd	16	bd	bd	2	12	17	16	13
Cd	1	1	bd	bd	5	8	6	6	8
Co	1	217	26	35	139	190	142	182	195
Ni	2	bd	20	38	20	50	86	56	61
Pb	6	1	94	81	10	51	49	48	47
Cu	38	51	83	62	47	29	40	35	27
Zn	22	35	65	113	46	42	56	54	51
Ba	3	9	519	403	43	94	40	75	34
Sr	bd	3	65	262	9	17	9	21	11
V	1	2	193	79	4	32	28	30	27
Cr	3	9	271	102	8	5	2	11	8
Zr	4	5	186	121	8	28	21	37	37

LOI = loss on ignition, bd = below detection. Total iron expressed as FeO.

Archaeum multi-element concentrations used for normalizations in Fig. 7, in ppm (Vinogradov, 1962; Taylor & McLennan, 1985): Se=0.6, Hg=0.4, Cd=0.3, Co=40, Ni=100, Pb=20, Cu=150, Zn=80, Ba=575, Sr=180, V=135, Cr=205, Zr=120.

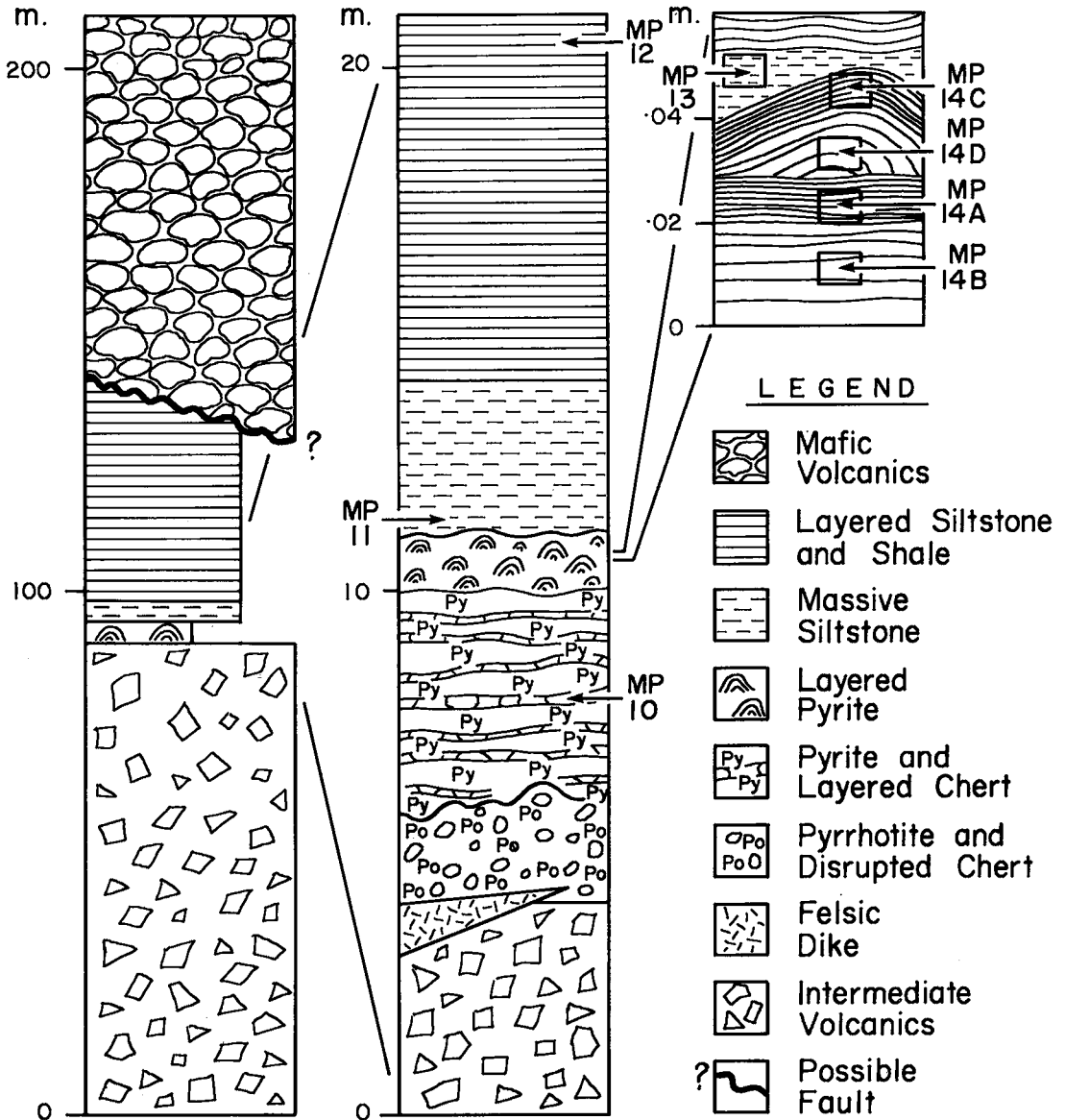


FIG. 2. Generalized stratigraphic sequence at the Morley pyrite occurrence, showing sample locations.

stone. Both halves exhibit thinning-upward successions of about 30 laminations (arrows in Fig. 3D). Thicker, basal, pyritic laminations in the successions are free of chert, clastic debris and carbon, whereas such material is common in the thinner overlying laminations. The top of the dome (Fig. 3A) is overlain by massive pyrite that thickens over the flanking depressions. The systematic change in lamination thickness shown in Figure 3D is common in the Morley pyrite. However, some pyritic layers (either

domed or flat) contain thin, monotonously similar laminations, and rare layers contain laminations that thicken upward.

Flat, finely laminated pyrite crusts, where traced laterally, commonly bend upward to form domal structures that may coalesce. Elsewhere, laminations in the domes intersect pyritic substrates sharply and at a high angle (Figs. 3C, 4A, 5C). Many colloform structures contain internal, low-angle discordant contacts, with individual layers or bundles of lamina-

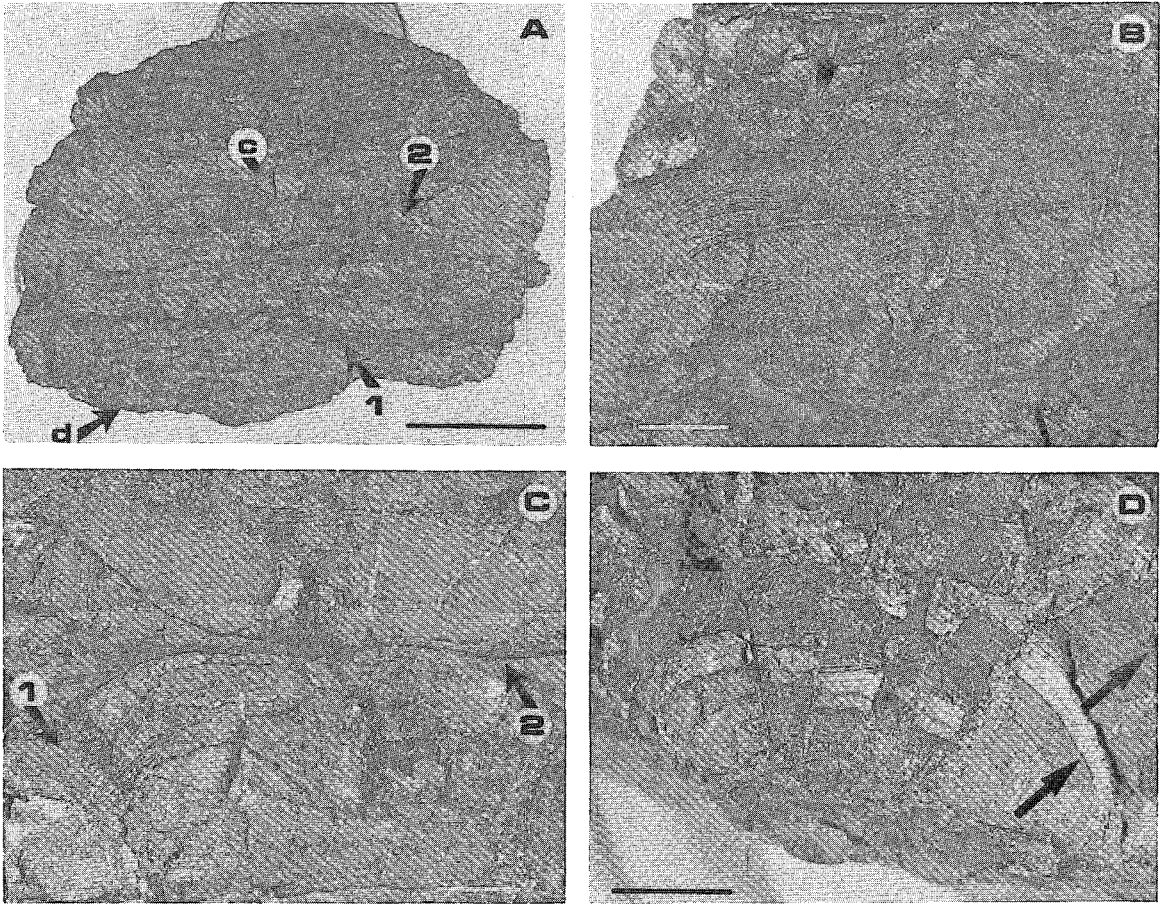


FIG. 3. Layering and lamination in pyritic hand samples A. Layering produced by dm-scale pyritic units separated by mm-scale carbonaceous slate partings (e.g., 1 and 2). Locations of structures in photographs 3c and 3d are shown (bar scale is 10 cm). B. Coalesced domal structures. Several smaller forms have merged during growth into one pyritic structure with two domal swellings but laterally continuous laminations. The pyrite structure is underlain and overlain by carbonaceous slate partings marked by arrows (bar scale is 1 cm). C. Colloform pyrite laminations in upper layer abut against a carbonaceous slate substrate (above arrow 2). The slate is much thinner above the lower pyritic structure, which has a smaller protrusion near its outer right edge. Lamination morphology in part of the lower colloform structure strongly resembles stromatolitic layering (bar scale is 0.5 cm). D. A large, microfaulted, colloform structure containing two upward-thinning successions (arrows). The base of the upper succession consists of three thick pyrite laminations resting on a thin carbonaceous slate lamination that caps the lower succession. Note pyrite veins along high-angle microfaults (scale is 1 cm).

tions truncated at angles of less than  $20^\circ$  by overlying layers. These truncations generally occur near the outer edge of a dome. The outer portion of some domes also exhibits smaller, pyritic overgrowths resembling potato eyes (Figs. 4B, 4C, 5C). In these overgrowths, laminations rise abruptly and at a high angle from the surface of the underlying domal structure; after a few millimeters, they bend sharply and become parallel to the underlying laminations of the dome. This produces a highly asymmetrical overgrowth.

The domal structures generally are oriented in a convex-upward direction, with only a minor percentage exhibiting reversed directions. The latter appear to have sagged downward into underlying muddy sediments. Some pyritic layers contain contorted laminations that in extreme cases are bent into small, recumbent folds. In addition to such small-scale load and slump structures, pyritic layers display variable degrees of brecciation, some of which may be post-burial. However, thin lenses ( $< 1$  cm thick) of pyritic gravel locally are present within the depressions

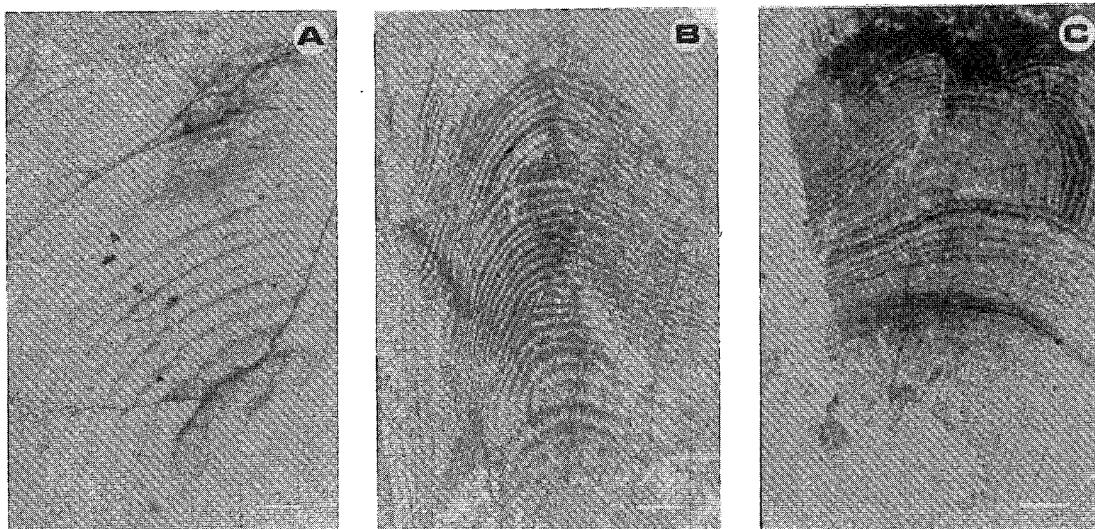


FIG. 4. Layering and lamination in pyritic polished samples (all scales are 2 mm). A. Colloform structure growing from a massive pyrite substrate. Lamination thickness decreases upward until the dark lamination, then increases in the upper third of the structure. B. Colloform structure with multiple growth-zones. The uppermost zones consist of sets of curving laminations that are concordant to highly discordant to each other, a feature common in the Morley occurrence. The fractured left side of the colloform structure is overlapped by a set of discordant pyritic laminations, strongly suggesting that the structure was brecciated and rotated prior to deposition of these laminations. C. Multiple, concordant to discordant growth-forms near the outer surface of a pyritic dome.

between colloform pyrite domes, together with hemispheroidal fragments, that probably represent toppled material from the domes. This indicates that at least some brecciation took place on the seafloor.

Pyrite veins are common throughout the whole chemical unit. Veins formed at the contacts between chert and pyrite layers commonly contain sphalerite along their margins (Figs. 5G, 5H). Chlorite, principally chamosite, fills interstitial areas in brecciated chert and pyrite (Fig. 5F). In some chloritic patches, chamositic cores are surrounded by more Mg-rich rims (FeO/MgO ranges from 0.87 to 0.41).

Near the tops of some pyrite laminations, iron oxides with intermixed carbon have replaced the pyrite, locally creating a boxwork texture (Figs. 6C, 6D). Iron oxides generally increase toward the tops

of individual laminations, reaching a maximum concentration immediately below either a sharp contact with the next pyrite-rich layer, or a gradational contact with a carbonaceous mudstone lamination. Boxwork textures and increased proportions of iron oxides and carbon are most common in the uppermost laminations of individual pyritic layers and domes.

#### GEOCHEMISTRY

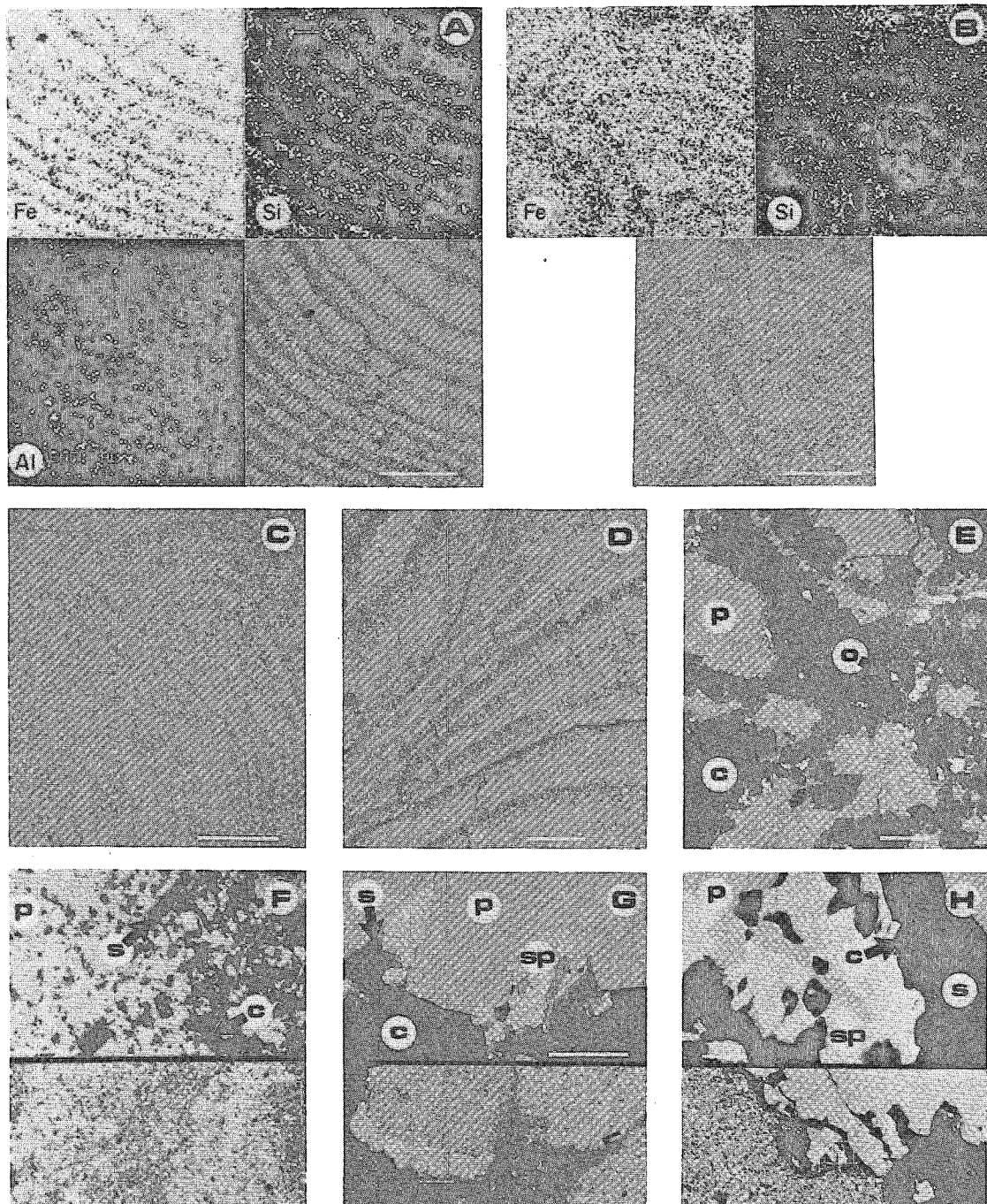
##### *Major and trace elements*

Nine samples representing the main lithologies at the Morley deposit (locations in Fig. 2) were analyzed for major and trace elements, rare-earth

FIG. 5. SEM back-scatter images of layering in pyritic polished and carbon-coated samples. A: Element distribution maps showing general decrease in Fe and increase in Si and Al toward the outer laminations (lower left of each view) of a colloform pyritic structure. A total spectrum image of the structure is also shown (scale is 1 mm). B: Element distribution maps of alternating layers rich in Fe and Si in two sharply discordant growth-zones (scale is 1 mm). C: Concordant to discordant growths on the outer part of a dome (scale is 1 mm). D: Compaction of layering under granular pyrite and brecciated pyrite (upper left) (scale is 1 mm). E: Iron oxides (o) replacing pyrite (p) and forming individual grains within chert (c) (scale is 0.2 mm). F to H: High magnification views in upper halves of photos show enlargements of small white boxes in lower halves. F: Chamosite (s) in brecciated pyrite (p) and chert (c) (scale is 0.05 mm). G: Sphalerite (sp) on the outer edge of a low-angle pyrite (p) vein. Chamosite (s) separates the sphalerite from the host carbonaceous chert (c) (scale is 0.1 mm). H: Sphalerite (sp) between massive pyrite and a mixture of chert (c), chamosite (s) and carbon (black areas). The rims of some chamosite grains have higher Mg contents (scale is 0.2 mm).

elements and sulfur isotopes (Table 1). The light and dark chert subsamples (MP10A and MP10B, respectively) contain >99% silica. Within the 5-cm-thick pyritic sequence, silica increases from the base to the top of both the laminated crust and the domal structure, whereas Fe decreases. Although some of this

silica is in the form of microscopic aluminosilicates (Al = 1.5–2.1%), Al and other cations show no consistent upward increase. This observation suggests an upward increase in free silica (as microscopic chert) within the laminated crust and domal structures.



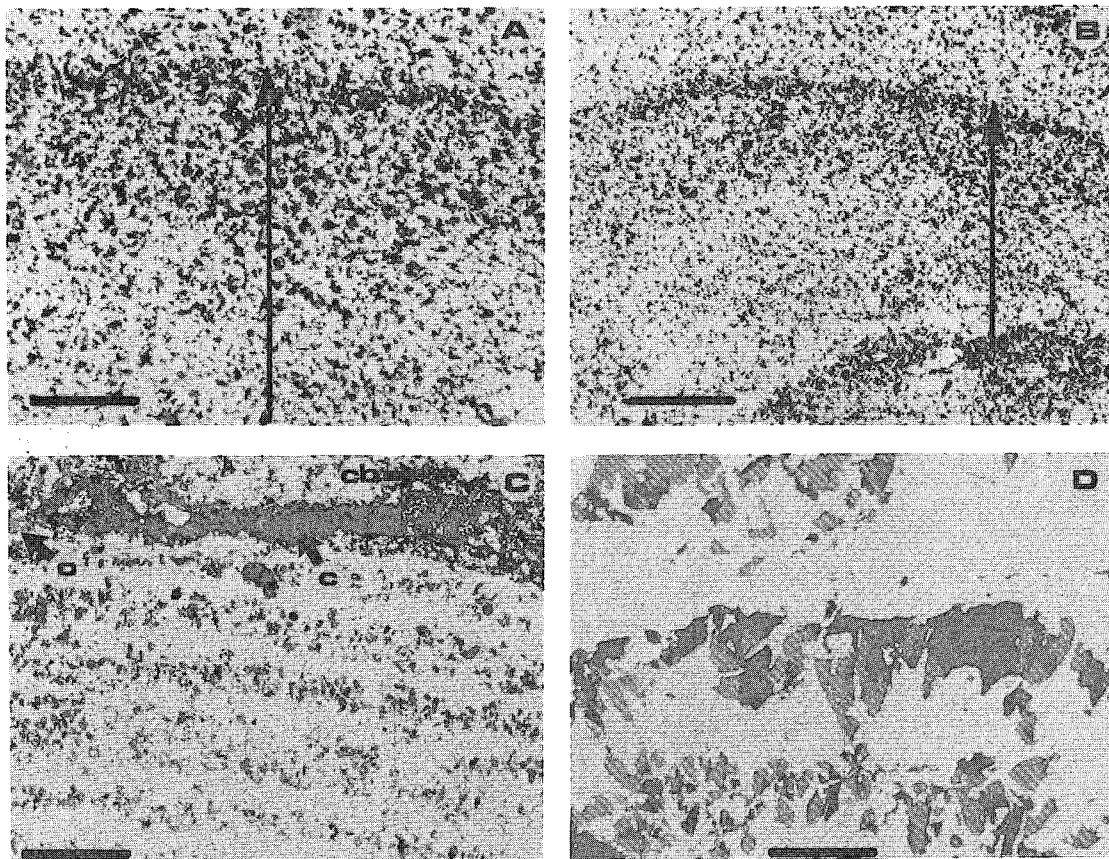


FIG. 6. Reflected light photomicrographs of mineralogical layering in pyritic (light) laminations. A: Chert and carbon content (dark) increases upward through a horizontal pyrite lamination (scale is 0.5 mm). B: Chert and carbon content increases upward through a colloform pyrite lamination (scale is 0.5 mm). C: Cherty mudstone (c), carbon (cb) and iron oxides (o) form the outer layer of a colloform structure (scale is 0.5 mm). D: Pyrite laminations alternating with boxwork-texture laminations rich in chert, iron oxides, and carbon with finely disseminated clastic material (scale bar is 0.05 mm).

The volcanic ash, which forms a massive siltstone layer above the Morley deposit, is felsic in composition, probably a dacite (MP11, Table 1). The distal turbidite from higher in the sequence (MP12) has a very similar composition, suggesting that it contains a large component of volcanoclastic material. Clastic material in the cherty black mudstone (MP13) appears to have a major-element composition close to that of the distal turbidite, as suggested by making a correction for silica addition, which would dilute the concentrations of other elements in the mudstone relative to the turbidite by a factor of about 2.4. The relatively immobile elements Ti and Al are in fact lower in the mudstone by factors of 2.8 and 2.6, respectively, consistent with Si addition. By contrast, the Fe content of the mudstone is twice the calculated "diluted" value of about 2%, suggesting addition of some hydrothermal iron during deposition.

The trace-element compositions of the nine samples, normalized to a composite shale, are shown in Figure 7. The elements on the left side of the *x* axis are typically associated with clastic material, whereas those on the right side are commonly of hydrothermal derivation. Overall, the four pyritic samples (MP14A–MP14D) are very similar in composition, with enrichments in the "hydrothermal" elements relative to average shale, but depletions in the "clastic" elements. Substitution of Cd, Hg and Se for sulfur in the pyrite probably accounts for the enrichment of these elements relative to shale. Lesser enrichments of Pb and Co may be due to trace amounts of galena and substitution for Fe in pyrite. The lower part of the laminated crust (MP14B) is somewhat enriched in Cu, Ni, Cd and Hg relative to the upper part (MP14A), but depleted in Cr, Sr, Ba and Zr relative to the upper part. This reflects a greater hydrothermal contribution to the lower por-

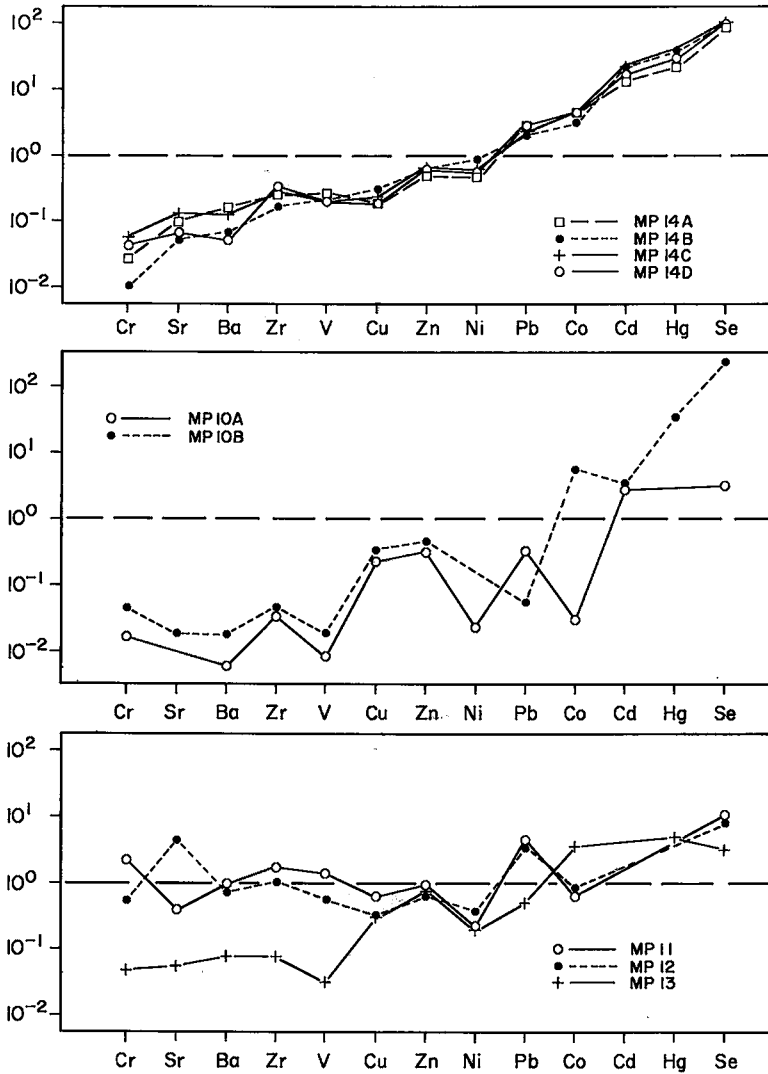


FIG. 7. Trace-element patterns for pyrite (MP14 subsamples), chert (MP10 subsamples), cherty mudstone (MP13), turbiditic slate (MP12) and volcanic ash (MP11). Zn, Cd, Hg and Se are normalized to average mudstone (Vinogradov 1962). Other elements are normalized to average Archean mudstone (Taylor & McLennan 1985). All data are reported in Table 1.

tion, and a greater clastic contribution to the upper portion. Similar relations hold for the lower (MP14D) and upper (MP14C) portions of the domal structure. The chert subsamples (MP10A,B) and the cherty mudstone (MP13) are generally enriched in the Cd, Hg and Se relative to shale, which can be attributed to finely disseminated pyrite within the chert. The distal turbidite (MP12) and the ash sample (MP11) generally plot close to average shale (dashed line), with the exception of higher Pb and Se contents.

#### Rare-earth elements (REE)

REE data on the Morley sample suite (Table 1) were obtained in the hope of identifying any hydrothermal signal. Sample concentrations were normalized to the REE composition of average Archean shale in order to recognize any nondetrital contribution to the sediments. The four pyritic subsamples, which have variable internal structures, display almost identical REE patterns, with positive La anomalies and small positive Eu<sup>2+</sup> anomalies (Fig.

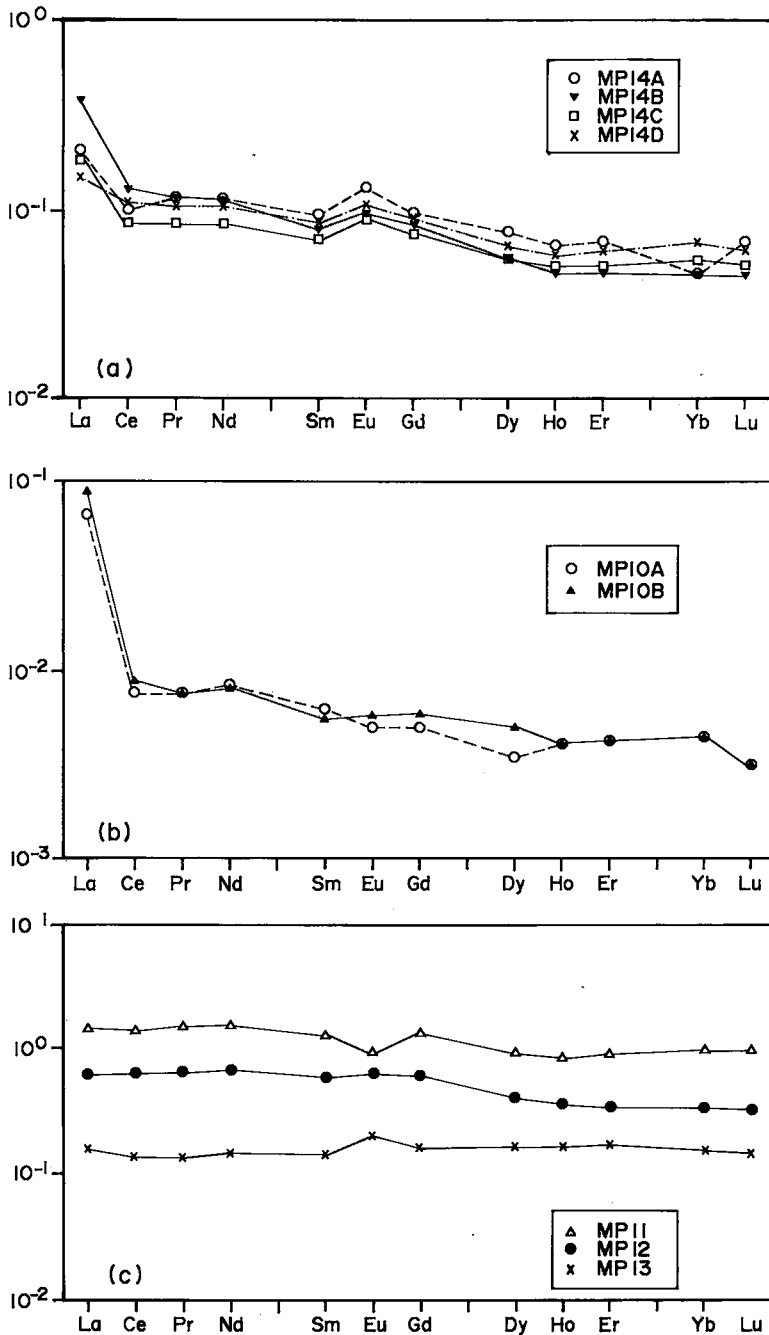


FIG. 8. Rare-earth-element patterns for pyrite (MP14 subsamples), chert (MP10 subsamples), cherty mudstone (MP13), turbiditic slate (MP12) and volcanic ash (MP11). REE values are normalized to average Archean mudstone (Taylor & McLennan 1985). All data are reported in Table 2.

8A). These data are consistent with earlier results on Morley pyrite (Barrett *et al.* 1988), and suggest a modest hydrothermal contribution during pyrite deposition. Positive Eu anomalies are displayed by

hydrothermal solutions discharging from modern seafloor vents (Michard *et al.* 1983, Campbell *et al.* 1988) and chemical sediments in the euxinic Atlantis II Deep in the Red Sea (Courtois & Treuil 1977). Precipitating solutions in these cases were sufficiently reduced that Eu existed as  $\text{Eu}^{2+}$  rather than in the trivalent state of the other REE. The  $p(\text{O}_2)$  range over which  $\text{Eu}^{2+}$  is stable varies according to temperature and pH (Sverjensky 1984), so that it is not possible to be more specific about solution conditions. The positive La anomalies of the Morley pyrite are rather enigmatic, as they have not been found in open-ocean hydrothermal systems, although they are present in some of the Atlantis II Deep chemical sediments (Courtois & Treuil 1977), as well as some iron-formation samples (Barrett *et al.* 1988).

The two chert subsamples from the Morley deposit have REE concentrations about an order of magnitude lower than the pyritic samples. The subsamples (light and dark bands) have almost identical patterns, with positive La anomalies but no Eu anomalies (Fig. 8B). One explanation is that discharging hydrothermal solutions carried no positive Eu anomaly, possibly because they had not experienced previous high-temperature interactions with basement rocks, which leads to the release of  $\text{Eu}^{2+}$  to reduced hydrothermal solutions (*cf.* Michard *et al.* 1983, Sverjensky 1984). Alternatively, high-temperature, reduced solutions became more oxidized prior to discharge, and lost any enrichment in  $\text{Eu}^{2+}$  in subsurface reactions. Solutions that are either relatively low-temperature or relatively oxidized might still be able to carry sufficient dissolved Si and La to account for chert precipitation and La enrichment in the chert. We suspect that the absence of a positive Eu anomaly in this chert sample is a localized feature. The existence of positive Eu anomalies in various facies of iron-formation sediments (Fryer 1977, Tu *et al.* 1985), including cherts from the same volcanic belt (Barrett *et al.* 1988), suggests that ambient seawater in the late Archean generally was much less oxygenated than at present.

The dacitic ash sample (MP11, Table 1) has a REE pattern typical of felsic volcanic rocks when normalized to chondritic values, that is, light REE enrichment and a small negative Eu anomaly (Taylor & McLennan 1985). The distal turbidite (MP12) has a near-flat pattern relative to that of average Archean mudstone (Fig. 8C), the latter of which has been interpreted as the result of more or less equal detrital contributions from mafic and felsic terranes (Taylor & McLennan 1985). The black cherty mudstone (MP13) has a pattern similar to that of the turbidite, with the exception of a small positive Eu anomaly, which may reflect the hydrothermal addition of silica (and some iron). None of these three mainly clastic sediments displays the La anomalies found in the pyritic and cherty precipitates.

### Sulfur isotopes

The 5-cm-thick pyritic interval at the Morley property has a relatively uniform sulfur isotopic composition (MP14, Table 2). Three of the four subsamples have  $\delta^{34}\text{S}$  values of 3.2–3.8‰, with the subsample from the top of colloform layer yielding a higher value, 4.6‰. Sulfur present in a dark chert layer has a higher  $\delta^{34}\text{S}$  value (5.0‰) than sulfur present as pyrite in the associated black mudstones (-1.4 and 2.5‰) and in the turbidite (2.8‰). All of these values lie within the range of values for late Archean sulfides of inferred magmatic derivation (see discussions in Lambert 1978, Ripley & Nicol 1981, Goodwin *et al.* 1985). At the Kingdom property, which lies in the same volcanic belt as the Morley occurrence, a thin pyrite-chert-mudstone iron formation contains colloform-lenticular pyrite with  $\delta^{34}\text{S}$  values of 5.3 and 8.6‰ (Table 2). Our sulfur isotope values for the whole data set are very similar to those of pyrite from late Archean turbidites and carbonaceous slates just south of Lake Superior, including slightly negative values for some of the slates (Ripley & Nicol 1981). These authors ascribed all of the  $\delta^{34}\text{S}$  range to seawater sulfate reduction at low temperatures, as the absence of associated volcanic rocks and the absence of massive sulfide layers seemed to rule out hot-spring activity. By contrast, the presence of locally massive pyrite layers at the Morley and Kingdom occurrences, together with the volcanic basements to the deposits, lead us to favor a hydrothermal-magmatic source for the sulfur in these samples. However, the presence of sulfide derived from reduction of seawater sulfate cannot be ruled out, as discussed below.

Numerous recent studies of massive sulfide deposits on the seafloor in open-ocean environments have yielded  $\delta^{34}\text{S}$  values in the 2 to 5‰ range (Bluth & Ohmoto 1988, Janecky & Shanks 1988, and references therein). These seafloor sulfides have become enriched in  $^{34}\text{S}$  through some combination of leaching of magmatic sulfide (~0‰) from the volcanic crust by hydrothermal solutions, and inorganic reduction of seawater sulfate in the solutions (the  $\delta^{34}\text{S}$  value of modern seawater is ~21‰). If modern hydrothermal systems can be used as a guide, then the  $\delta^{34}\text{S}$  values of Archean massive sulfides within the positive part of the inferred "magmatic" range (~0 to 5‰) probably also contain a component of sulfate-derived sulfide. At Morley, the massive pyrite layers may represent deposition from such a fluid (in the 3 to 5‰ range). In euxinic and restricted bottom-waters fed by hydrothermal input, such as in the Atlantis II Deep,  $\delta^{34}\text{S}$  values of sulfides formed as brine pool precipitates and in epigenetic veins range from ~1 to 15‰ and from 4.5 to 10.5‰, respectively (Shanks & Bischoff 1980, Zierenberg & Shanks 1988), with average values of ~5.5‰ in both cases. The higher values within these

TABLE 2. RARE-EARTH-ELEMENT CONCENTRATIONS AND SULFUR ISOTOPIC COMPOSITION OF PYRITIC SULFIDES AND ASSOCIATED LITHOLOGIES, MORLEY OCCURRENCE, NORTHWESTERN ONTARIO

REE	MP10A light chert	MP10B dark chert	MP11 ash	MP12 turb. slate	MP13 cherty mudst.	MP14A pyrite	MP14B pyrite	MP14C pyrite	MP14D pyrite	MP14A (R)
La	1.33	1.75	28.7	12.4	3.08	4.16	7.66	3.72	2.99	4.09
Ce	0.326	0.380	58.7	26.8	3.74	4.23	5.47	3.70	4.73	4.47
Pr	0.038	0.037	7.40	3.26	0.663	0.522	0.370	0.428	0.338	0.311
Nd	0.174	0.163	31.3	13.9	2.89	2.16	2.28	1.75	2.16	2.10
Sm	0.025	0.022	5.22	2.36	0.567	0.393	0.336	0.294	0.357	0.361
Eu	0.006	0.007	1.15	0.777	0.238	0.160	0.124	0.112	0.133	0.153
Gd	0.017	0.020	4.71	2.07	0.552	0.342	0.305	0.264	0.315	0.340
Tb	0.003	0.003	0.593	0.266	0.091	0.048	0.036	0.037	0.040	0.044
Dy	0.012	0.017	3.24	1.41	0.559	0.270	0.196	0.194	0.230	0.242
Ho	0.003	0.003	0.655	0.269	0.118	0.051	0.036	0.038	0.045	0.050
Er	0.009	0.009	1.96	0.729	0.355	0.150	0.102	0.112	0.138	0.144
Tm	0.001	0.001	0.298	0.107	0.049	0.022	0.015	0.018	0.021	0.021
Yb	0.009	0.009	1.98	0.660	0.305	0.141	0.097	0.113	0.141	0.138
Lu	0.001	0.001	0.315	0.099	0.046	0.022	0.015	0.017	0.020	0.020
$^{34}\text{S}/^{32}\text{S}$ values (‰)										
	MP12 turb. slate	MP13 cherty mudst.	MP14A pyrite	MP14B pyrite	MP14C pyrite	MP14D pyrite	MP3 pyritic mudst.	MP4 pyritic chert	K1 pyrite	K2 pyrite
	+2.82 ±0.24	-1.40 ±0.23	+3.38 ±0.26	+3.24 ±0.21	+4.59 ±0.39	+3.75 ±0.14	+2.5 ±0.2	+5.0 ±0.2	+8.6 ±0.2	+5.3 ±0.2

Rare-earth elements: all concentrations in ppm. (R): replicates.

Archean mudstone concentrations used for normalizations in Fig. 8, in ppm (Taylor & McLennan, 1985):

La=20, Ce=42, Pr=4.9, Nd=20, Sm=4.0, Eu=1.2, Gd=3.4, Dy=3.4, Ho=0.74, Er=2.1, Yb=2.0, Lu=0.31

Sulfur isotopes: all samples analyzed by direct combustion method except Morley samples MP3 and MP4, which were analyzed following Kiba extraction method. K1 and K2 are samples from Kingdom property. Samples MP10A, MP10B and MP11: insufficient  $\text{H}_2\text{S}$  gas for analysis.

ranges are thought to reflect an increased proportion of sulfide derived from inorganic reduction of dissolved sulfate by ferrous iron in basalts or in the ascending hydrothermal solution (Zierenberg & Shanks 1988). By analogy, the  $\delta^{34}\text{S}$  range in our Archean data set, excluding the one slightly negative value, could be explained by mixtures of magmatic and seawater-derived sulfide. The negative value might indicate that minor bacterial reduction of sulfate occurred.

At the Morley deposit, the presence of carbonaceous mudstone bands, and of abundant carbon near the tops of pyritic laminations, does suggest that some organic material was present near sites of pyrite deposition. Unfortunately, neither the  $\delta^{34}\text{S}$  value of seawater sulfate in the late Archean nor the concentration of dissolved sulfate are well constrained (cf. Ripley & Nicol 1981, Cameron 1982). Thus the ranges of sulfur isotopic trends to be expected for a particular process cannot be estimated reliably. For  $\delta^{34}\text{S}$  values in the  $\sim 2$  to 6‰ range in particular, we cannot estimate the sulfur contributions from a "hydrothermal" fluid with a major (but not necessarily total) contribution of magmatic sulfide on the one hand, and inorganically or organically reduced seawater sulfate on the other.

## MODERN HYDROTHERMAL SYSTEMS

### Atlantis II Deep

Deposits of metalliferous muds ranging from the oxide to the silicate to the sulfide facies occur within temperature- and salinity-stratified brine deeps occupying topographic depressions along the spreading axis of the Red Sea (Degens & Ross 1969). In the Atlantis II Deep, the metalliferous horizons form

blankets up to several meters in thickness that extend for kilometers along strike. The sediments consist of well-layered and laminated muds, indicative of quiet accumulation without current activity. The two brine layers from which most of the metals precipitate are devoid of oxygen (Hartmann 1985). A hydrothermal source for the deepest and warmest bottom-water layer (44–56°C) is apparently located in the southwest part of the basin, where fluid inclusions from veins in the underlying sediments yield temperatures of up to  $\sim 400^\circ\text{C}$  (Ramboz *et al.* 1988). Precipitation of the various metalliferous facies occurs in response to the different Eh–pH–*T* conditions that exist in the brine layers and the overlying normal seawater (Bischoff 1969).

The mm-scale horizontal lamination commonly found in the pyritic, cherty and slaty layers at the Morley is similar to that found in the metalliferous muds of the Atlantis II Deep, including the sulfide-facies muds. The latter muds, like the main Morley pyrite zone, also contain thin layers and mm-scale laminations of detrital (pelagic) material (Ross & Degens 1969). The thickness of the Morley deposit is similar to the sulfide-facies horizon in the Atlantis II Deep, as is its location immediately above volcanic rocks. The carbonaceous mudstones associated with the Morley pyrite indicate an overall reducing environment, although the Eh oscillated during pyrite deposition, as shown by the partly oxidized sulfide laminations in the upper portions of some colloform pyritic structures. The layered chert located mostly below the pyritic capping of the deposit may reflect a much higher ratio of Si to Fe in early hydrothermal fluids (we also infer precipitation of this chert from less reduced solutions). Although siliceous ooze does not occur in association with sulfide-facies muds in the Atlantis II Deep, a silica-rich slurry has precipitated at the sediment–seawater interface (Danielsson *et al.* 1980).

### Open-ocean spreading axes

Sulfide-rich deposits are forming from modern "black smokers" at spreading axes on the ocean floor, particularly in the East Pacific (Corliss *et al.* 1979, Francheteau *et al.* 1979, RISE 1980), but also in the Atlantic (Rona *et al.* 1986, Thompson *et al.* 1988). The smokers are located above vents that discharge hot fluids (mostly  $\sim 350^\circ\text{C}$ ) rich in dissolved metals (Edmond *et al.* 1982). Massive sulfides precipitate within and immediately around the discharge orifices as the chimneys grow upward; sulfates and amorphous silica also are important phases at some vents. As the hydrothermal fluid mixes with the cold, oxidized seawater, metallic sulfides and oxide-hydroxides precipitate within a buoyant plume of black smoke (Feely *et al.* 1987). However, most of the smoke does not fall back as sediment in the

vicinity of the chimneys (Converse *et al.* 1984), but is carried away from the vent site(s) by bottom currents.

Modern vent systems appear to exhibit episodic hydrothermal behavior, with scales of episodicity ranging from days to tens of years (Macdonald *et al.* 1980, Lalou & Brichet 1982). Large-scale fluctuations are caused by magma cooling and recharge cycles operating at depth; small-scale cycles are the result of changes in the plumbing systems of the mounds themselves as vents are sealed by precipitating material, or as cold seawater breaks through the mound base (Rona 1984).

Colloform, cm-scale pyritic structures have been reported from chimneys on the Juan de Fuca Ridge (Koski *et al.* 1984, p. 936), but their subvertical layering differs profoundly from that at the Morley occurrence, where mud drapes and other evidence indicate that the pyrite was deposited on a near-horizontal bottom. Hékinian & Fouquet (1985) described minute ( $\ll 1$  mm across) colloform pyritic structures forming from a presently low-temperature, diffuse hydrothermal system at 13°N on the EPR. These authors noted (p. 241) that concretions of colloform pyrite were overlain by pyrite partially altered into goethite. On the Palinuro Seamount in the Tyrrhenian Sea, sulfide crusts containing "spherulitic" pyrite are interbedded with ooze of organic and volcanic origin, and surface crusts "are generally blackened and are sometimes associated with thin reddish layers produced by oxidation" (Minniti & Bonavia 1984). The latter two occurrences are analogous to the seafloor oxidation of the upper surfaces of some of the Morley pyritic structures.

On the Mid-Atlantic ridge, hydrothermal sulfide chimneys have been subjected to erosion, and the talus transported at least 1 km from the vent sites, producing hydrothermal layers ranging from sub-mm- to cm-scale in thickness that are interlayered with normal pelagic sediments (Metz *et al.* 1988). However, there is no evidence in the Morley deposit for a detrital origin for the laminated pyrite layers. In the central Atlantic, pyrite concretions of inferred hydrothermal origin have been dredged from the Romanche fracture zone (Bonatti *et al.* 1976). These discoidal concretions display a number of features common to the Morley pyrite domes, including cm-scale width, internal layering ("concentric growth rings"), oxidation to iron-hydroxide-rich exteriors, and the presence of clastic grains in an iron-hydroxide-rich matrix (Bonatti *et al.* 1976). The authors, however, did not speculate on the origin of the banding in the concretions.

#### THE MORLEY HYDROTHERMAL SYSTEM

The fine-grained nature of the dark mudstones associated with the Morley occurrence denotes quiet

accumulation below storm wave-base. Pelagic rain-out of mud, which formed the clast-bearing laminations within pyritic layers, was periodically overwhelmed by chemical precipitation of pyrite or chert. Layering in the pyritic beds reflects three scales of episodicity, which from shortest to longest duration are represented by: i) alternating pyrite-rich and clast- and carbon-rich laminations; ii) cm-scale, thinning upward cycles of these alternating laminations, and iii) interbedded pyritic and carbonaceous mudstone layers (the former either parallel-laminated or colloform). In addition, there is a passage from chert-rich to pyrite-rich precipitates over the entire chemical unit. These various sequences are interpreted in terms of fluctuations in seafloor hydrothermal discharge, which was diffuse rather than focussed at a vent site. Each pyritic lamination reflects an individual hydrothermal pulse. As a short-term hydrothermal event waned, more chert was precipitated. After hydrothermal activity ceased, limited oxidation of the exposed upper surface of the pyrite-rich laminations ensued on the seafloor (unless another hydrothermal pulse followed almost directly). At this time, some organic carbon and clastic mud also accumulated. The presence of bundles of laminations, in which pyritic laminations thin upward but the proportion of intervening detritus increases, suggests a medium-term, oscillatory waning of hydrothermal-activity (with superimposed short-term pulses). Longer-term cessations in hydrothermal activity are reflected by the presence of thin, generally carbonaceous mudstones interbedded with the pyritic layers.

Laminated, sulfide-rich sediments analogous to the Morley deposit are not developed around modern hydrothermal vent-sites in the open ocean. The main reason seems to be that modern chemical precipitates are dispersed too widely throughout bottom waters, and settle at too great a distance to record anything but very long-term variations in hydrothermal activity (*e.g.*, the hydrothermal history illustrated by the DSDP Leg 92 sediments; Rea & Leinen 1986). Short-term variations will be recorded if precipitates from an individual pulse of hydrothermal activity are not extensively diluted by bottom currents, and can accumulate on the basin floor without disturbance. We speculate that the Morley sulfides were precipitated from a bottom-water layer that was confined to a stagnant sub-basin. If discharging hydrothermal solutions at the Morley had salinities close to that of the bottom-water layer, temperatures would have been fairly low in order to reduce discharge rates (*i.e.* lower the buoyancy) and thereby stabilize such a bottom layer. Any calculation of absolute densities should consider the possibility that ambient seawater in the Archean was warmer and less saline than modern seawater (Maisonneuve 1982).

The structures present in the colloform and irregu-

larly laminated pyrite are difficult to explain solely by rainout of chemical precipitates (and clastic mud) from above. Rainout would not produce the dome-shaped mounds or gravitationally unstable features such as the discordant pyritic growths. The geometry of the laminations in some domes strongly suggests the existence of organic mats that influenced sedimentation by trapping fine-grained pyritic rainout within domal to irregular bottom structures. The Morley structures are similar to those found in both modern and ancient stromatolites (stromatolite morphology is reviewed in Logan *et al.* 1964). Modern stromatolites, however, are restricted to the photic zone (tens of meters depth), whereas the Morley pyritic structures are associated with a distal sequence of mudstones and turbidites indicative of deeper water.

An alternative organic influence may have been microbial mats, which are well documented in recent fields of black smokers (Jannasch & Wirsén 1981, Jannasch 1984). Microbial activity associated with hydrothermal venting on the Archean seafloor has been postulated for certain localities (*e.g.*, Goodwin *et al.* 1985). If microbial mats were locally developed near vent sites at the Morley, such mats must have existed in association with pyrite deposition and therefore been tolerant of low levels of oxygen. The carbon in the carbonaceous mudstones and within the pyritic laminations may represent relics of such former organic activity. Pyritic carbonaceous slates from the Helen mine in the Wawa greenstone belt, also of late Archean age, have a negative carbon isotope ratio, interpreted by Goodwin *et al.* (1985) to result from the action of sulfate-reducing bacteria. In our interpretation of the Morley deposit, the lamination and layering of pyrite largely reflect variations in hydrothermal input at a relatively deep-water site, rather than variations in biogenic activity in the photic zone (*e.g.*, daily to seasonal growth-cycles). Deep-water organic mats, presumably chemosynthetic in nature, could have provided the substrate on which the iron sulfide precipitates accumulated, although we cannot assess whether they could have produced the observed range of textures within the pyritic sequence. Finally, if organic mats extracted iron from bottom waters during periods of increased hydrothermal supply, rather than simply acting as a substrate to fallout material, saturation of bottom waters with respect to pyrite would not be required. Furthermore, if organic mats were able to reduce seawater sulfate during iron sulfide precipitation, the problem of simultaneous transport of iron and sulfur in relatively low-temperature hydrothermal solutions could be overcome. As a general model, we suggest that sulfide-facies iron formation characterized by irregularly laminated to domal pyrite and intimately associated carbonaceous mudstones reflects the presence of organic mats, and therefore prox-

imity to a relatively low-temperature and diffuse system of vents. Cm-scale layers of parallel-laminated pyrite may represent bottom-layer fallout distal to venting fluids, possibly the result of supersaturation of the layer with respect to iron sulfide (no organic influence). In both cases, however, the cm- to mm-scale banding in the pyrite is directly or indirectly the result of episodic injections of iron-rich solutions into a euxinic bottom-water layer.

#### ACKNOWLEDGEMENTS

We are particularly grateful to the Thunder Bay staff of the Ministry of Northern Development and Mines (Mines and Mineral Division) for helpful discussions and information on occurrences of iron formation in the study area. Useful comments and suggestions on an earlier version of the manuscript were provided by two anonymous reviewers. This research was supported in part by the Natural Sciences and Engineering Research Council of Canada and by the National Environmental Research Council of Britain.

#### REFERENCES

- BARRETT, T.J., FRALICK, P.W. & JARVIS, I. (1988): Rare-earth-element geochemistry of some Archean iron-formations north of Lake Superior, Ontario. *Can. J. Earth Sci.* **25**, 570-580.
- BISCHOFF, J.L. (1969): Red Sea geothermal brine deposits: their mineralogy, chemistry, and genesis. *In* Hot Brine and Recent Heavy Metal Deposits in the Red Sea (E.T. Degens & D.A. Ross, eds.). Springer-Verlag, New York (368-401).
- BLUTH, G.J. & OHMOTO, H. (1988): Sulfide-sulfate chimneys on the East Pacific Rise, 11° and 13°N latitudes. II. Sulfur isotopes. *Can. Mineral.* **26**, 505-515.
- BONATTI, E., HONNOREZ-GUERSTEIN, M.B., HONNOREZ, J. & STERN, C. (1976): Hydrothermal pyrite concretions from the Romanche Trench (equatorial Atlantic): metallogenesis in oceanic fracture zones. *Earth Planet. Sci. Lett.* **32**, 1-10.
- CAMERON, E.M. (1982): Sulphate and sulphate reduction in early Precambrian oceans. *Nature* **296**, 145-148.
- CAMPBELL, A.C., PALMER, M.R., KLINKHAMMER, G.P., BOWERS, T.S., EDMOND, J.M., LAWRENCE, J.R., CASEY, J.F., THOMPSON, G., HUMPHRIS, S., RONA, P. & KARSON, J.A. (1988): Chemistry of hot springs on the Mid-Atlantic Ridge. *Nature* **335**, 514-519.
- CONVERSE, D.R., HOLLAND, H.D. & EDMOND, J.M. (1984): Flow rates in the axial hot springs of the East Pacific Rise (21°N): implications for heat budget and

- the formation of massive sulphide deposits. *Earth Planet. Sci. Lett.* **69**, 159-175.
- CORLISS, J.B., DYMOND, J., GORDON, L.I., EDMOND, J.M., VON HERZEN, R.P., BALLARD, R.D., GREEN K., WILLIAMS, D., BAINBRIDGE, A., CRANE, K. & VAN ANDEL, T.H. (1979): Submarine thermal springs on Galapagos Rift. *Science* **203**, 1073-1083.
- COURTOIS, C. & TREUIL, M. (1977): Distribution des terres rares et de quelques éléments en trace dans les sédiments récents des fosses de la Mer Rouge. *Chem. Geol.* **20**, 57-72.
- DANIELSSON, L.-G., DYRSSEN, D. & GRANÉLI, A. (1980): Chemical investigations of Atlantis II and Discovery brines in the Red Sea. *Geochim. Cosmochim. Acta* **44**, 2051-2065.
- DEGENS, E.T. & ROSS, D.A., eds. (1969): *Hot Brine and Recent Heavy Metal Deposits in the Red Sea*. Springer-Verlag, New York.
- EDMOND, J.M., VON DAMM, K.L., MCDUFF, R.E. & MEASURES, C.I. (1982): Chemistry of hot springs on the East Pacific Rise and their effluent dispersal. *Science* **297**, 187-191.
- FEELY, R.A., LEWISON, M., MASSOTH, G.J., ROBERT-BALDO, G., LAVELLE, J.W., BYRNE, R.H., VON DAMM, K.L. & CURL, H.C., JR. (1987): Composition and dissolution of black smoker particulates from active vents on the Juan de Fuca Ridge. *J. Geophys. Res.* **92**, 11347-11363.
- FRANCHETEAU, J., NEEDHAM, H.D., CHOUKROUNE, P., JUTEAU, T., SEGURET, M., BALLARD, R.D., FOX, P.J., NORMARK, W., CARRANZA, A., CORDOBA, D., GUERRERO, J., RANGIN, C., BOUGAULT, H., CAMBON, P. & HÉKINIAN, R. (1979): Massive deep-sea sulfide ore deposits discovered on the East Pacific Rise. *Nature* **277**, 523-528.
- FRYER, B.J. (1977): Rare earth evidence in iron-formations for changing Precambrian oxidation states. *Geochim. Cosmochim. Acta* **41**, 361-367.
- GOODWIN, A.M. (1964): Geochemical studies at the Helen Iron Range. *Econ. Geol.* **59**, 684-718.
- \_\_\_\_\_, THODE, H.G., CHOU, C.-L. & KARKHANSIS, S.N. (1985): Chemostratigraphy and origin of the late Archean siderite-pyrite-rich Helen Iron Formation, Michipicoten belt, Canada. *Can. J. Earth Sci.* **22**, 72-84.
- GROSS, G.A. (1965): Geology of iron deposits in Canada. 1. General geology and evaluation of iron deposits. *Geol. Surv. Can., Econ. Geol. Rep.* **22**.
- \_\_\_\_\_ (1983): Tectonic systems and the deposition of iron-formation. *Precambrian Res.* **20**, 171-187.
- HARCOURT, G.A. & BARTLEY, M.W. (1939): The Schreiber area. *Ont. Dep. Mines, Ann. Rep.* XLVII, Part IX.
- HARTMANN, M. (1985): Atlantis-II Deep geothermal brine system. Chemical processes between hydrothermal brines and Red Sea deep water. *Marine Geol.* **64**, 157-177.
- HÉKINIAN, R. & FOUQUET, Y. (1985): Volcanism and metallogenesis of axial and off-axial structures on the East Pacific Rise near 13°N. *Econ. Geol.* **80**, 221-249.
- JAMES, H.L. (1966): Chemistry of the iron-rich sedimentary rocks. *U.S. Geol. Surv., Prof. Pap.* 440W.
- JANECKY, D.R. & SHANKS, W.C., III (1988): Computational modelling of chemical and sulfur isotopic reaction processes in seafloor hydrothermal systems: chimneys, massive sulfides, and subjacent alteration zones. *Can. Mineral.* **26**, 805-825.
- JANNASCH, H.W. (1984): Microbial processes at deep sea hydrothermal vents. In *Hydrothermal Processes at Seafloor Spreading Centers* (P.A. Rona, K. Bostrom, L. Laubier & K.L. Smith, Jr., eds.). NATO Conf. Series, IV, *Marine Sciences* **12**, Plenum Press, New York, (677-709).
- \_\_\_\_\_ & WIRSEN, C.O. (1981): Morphological survey of microbial mats near deep-sea thermal vents. *Appl. Environ. Microbiol.* **41**, 528-538.
- JARVIS, I. & JARVIS, K.E. (1985): Rare-earth element geochemistry of standard sediments: a study using inductively coupled plasma spectrometry. *Chem. Geol.* **53**, 335-344.
- JARVIS, K.E. (1988): Inductively coupled plasma mass spectrometry: a new technique for the rapid or ultra-trace level determination of the rare-earth elements in geological materials. *Chem. Geol.* **68**, 31-39.
- KOSKI, R.A., CLAGUE, D.A. & OUDIN, A. (1984): Mineralogy and chemistry of massive sulfide deposits from the Juan de Fuca Ridge. *Geol. Soc. Am. Bull.* **95**, 930-945.
- LALOU, C. & BRICHET, E. (1982): Ages and implications of East Pacific Rise sulphide deposits at 21°N. *Nature* **300**, 169-171.
- LAMBERT, I.B. (1978): Sulphur-isotope investigations of Archean mineralization and some implications concerning geobiochemical evolution. In *Archean Cherty Metasediments: Their Sedimentology, Micropalaeontology, Biogeochemistry and Significance to Mineralization*. Publ. Geol. Dep. & Extension Services, Univ. Western Aust. **2**, 45-56.
- LOGAN, B.W., REZKA, R. & GINSBURG, R.N. (1964): Classification and environmental significance of algal stromatolites. *J. Geol.* **72**, 68-83.
- MACDONALD, K.C., BECKER, K., SPEISS, F.N. & BALLARD, R.D. (1980): Hydrothermal heat flux of the

- “black smoker” vents on the East Pacific Rise. *Earth Planet. Sci. Lett.* **48**, 1-7.
- MAISONNEUVE, J. (1982): The composition of the Precambrian ocean waters. *Sediment. Geol.* **31**, 1-11.
- METZ, S., TREFRY, J.H. & NELSON, T.A. (1988): History and geochemistry of a metalliferous sediment core from the Mid-Atlantic Ridge at 26°N. *Geochim. Cosmochim. Acta* **52**, 2369-2378.
- MICHARD, A., ALBARÈDE, F., MICHARD, G., MINSTER, J.F. & CHARLOU, J.L. (1983): Rare-earth elements and uranium in high-temperature solutions from East Pacific Rise hydrothermal vent field (13°N). *Nature* **303**, 795-797.
- MINNITI, M. & BONAVIA, F.F. (1984): Copper-ore grade hydrothermal mineralization discovered in a seamount in the Tyrrhenian Sea (Mediterranean): is the mineralization related to porphyry coppers or to base metal lodes? *Marine Geol.* **59**, 271-282.
- RAMBOZ, C., OUDIN, E. & THISSE, Y. (1988): Geysertype discharge in Atlantis II Deep, Red Sea: evidence of boiling from fluid inclusions in epigenetic anhydrite. *Can. Mineral.* **26**, 765-786.
- REA, D.K. & LEINEN, M. (1986): Neogene controls on hydrothermal activity and paleoceanography of the Southeast Pacific Ocean. *Initial Rep. Deep Sea Drilling Project* **92**, 597-617.
- RIPLEY, E.M. & NICOL, D.L. (1981): Sulfur isotope studies of Archean slate and graywacke from northern Minnesota: evidence for the existence of sulfate reducing bacteria. *Geochim. Cosmochim. Acta* **45**, 839-846.
- RISE PROJECT GROUP (1980): East Pacific Rise: hot springs and geophysical experiments. *Science* **207**, 1421-1433.
- RONA, P.A. (1984): Hydrothermal mineralization at seafloor spreading centres. *Earth-Sci. Rev.* **20**, 1-104.
- \_\_\_\_\_, KLINKHAMMER, G., NELSON, T.A., TREFRY, J.H. & ELDERFIELD, H. (1986): Black smokers, massive sulfides and vent biota at the Mid-Atlantic Ridge. *Nature* **321**, 33-37.
- ROSS, D.A. & DEGENS, E.T. (1969): Shipboard collection and preservation of sediment samples collected during Chain 61 from the Red Sea. In *Hot Brine and Recent Heavy Metal Deposits in the Red Sea* (E.T. Degens & D.A. Ross, eds.). Springer-Verlag, New York (363-367).
- SCHNIEDERS, B.R. (1987): *Geology and Depositional Environment of Sulphide Facies Iron Formation in the Lower Steel River-Little Steel Lake Area, Terrace Bay, Northwestern Ontario*. M.Sc. thesis, Lakehead University, Thunder Bay, Ontario.
- SHANKS, W.C., III & BISCHOFF, J.L. (1980): Geochemistry, sulfur isotope composition, and accumulation rates of Red Sea geothermal deposits. *Econ. Geol.* **75**, 445-459.
- SVERJENSKY, D.A. (1984): Europium redox equilibria in aqueous solutions. *Earth Planet. Sci. Lett.* **67**, 70-78.
- TAYLOR, S.R. & MCLENNAN, S.M. (1985): *The Continental Crust: its Composition and Evolution*. Blackwell Scientific Publications, Oxford, U.K.
- THOMPSON, G., HUMPHRIS, S.E., SCHROEDER, B., SULANOWSKA, M. & RONA, P.A. (1988): Active vents and massive sulfides at 26°N (TAG) and 23°N (Snakepit) on the Mid-Atlantic Ridge. *Can. Mineral.* **26**, 697-711.
- TU GUANGZHI, ZHAO ZHENHUA & QIU YUZHUO (1985): Evolution of Precambrian REE mineralization. *Precambrian Res.* **27**, 131-151.
- VINOGRADOV, A.P. (1962): Average contents of chemical elements in the principal types of igneous rocks of the earth's crust. *Geochemistry*, 641-664.
- ZIERENBERG, R.A. & SHANKS, W.C. III (1988): Isotopic studies of epigenetic features in metalliferous sediment, Atlantis II Deep, Red Sea. *Can. Mineral.* **26**, 737-753.

Received July 28, 1987, revised manuscript accepted June 28, 1989.